Print Noise Diagnoses through Correlation Analyses

Palghat Ramesh, Peter Paul and Eric Gross; Xerox Research Center Webster, Webster, New York

Abstract

In recent years, there has been considerable interest in color stability of printed output from a marking engine. In general, colors can vary within a page, page-to-page, job-to-job, and engine-to-engine. Diagnosing the nature and sources of the color variability can help lead to approaches to reduce variability, such as improved subsystem components and improved process controls. In this paper, we discuss a methodology to diagnose the root causes of color variability.

Introduction

Color stability is a major requirement in the printing industry [1]. Variability of color within a page, between pages within a job, and between jobs within a marking engine is an important print quality metric. In many cases, color can change over time, due to changes in operating conditions, such environment, customer area coverage, paper type etc. or as printer components age. It is of considerable interest to understand the sources of color variability in a printer.

In color xerographic printing, an image undergoes several transformations, from an electrostatic latent image, to a toner mass image, to a fused image. Temporal variations to the image can be introduced at each of these stages. Typical types of variation can include drift, structured noises such as banding or streaks as well as unstructured noise. In many xerographic systems, closed loop controls are used to mitigate color stability [2]. Sensors are used to monitor toner density on a photoconductor or intermediate belt and electrostatic voltages or laser power is adjusted to regulate them. The process controls are typically designed to mitigate slow shifts in toner density that happen over time scales of tens to hundreds of prints. However, structured and unstructured noises, variations in processes downstream of the sensors such as in transfer and fusing, as well as rapid transients such as due to a sudden toner dispense event during low area coverage printing, can cause significant color shifts even in the presence of process controls.

In this paper, we discuss methodologies to diagnose color variation in printers. Voltage, mass, and color sensors are used to capture the intermediate as well as the final image states. We describe the use of time series analyses to obtain correlations among these states. We discuss the use of such analyses to help identify sources of color variability, and to suggest potential approaches to minimize them.

Methodology

Figure 1 shows a schematic of a xerographic color printer instrumented with sensors to capture intermediate and final image states. For example, electrostatic voltmeters (ESV) on photoconductor drums can be used to capture the latent image, toner density sensors on the intermediate belt to capture the developed toner image and color sensors to measure the color of fused prints. In general, the more the intermediate image states that can be captured reliably, the more the information that can be gleaned from the correlation analyses. Since most sensors tend to be point sensors, the signal to noise of the analyses can be improved by collocation of the sensors in the cross process direction.

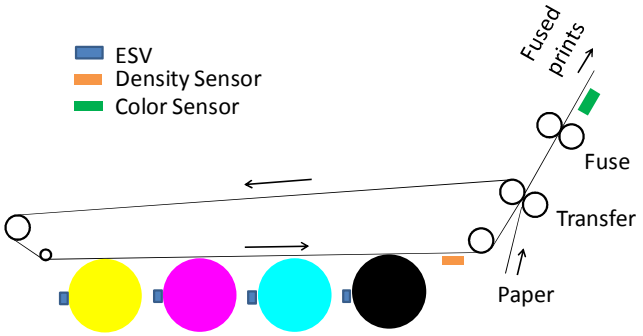

Figure 1: Schematic of a color printer instrumented with sensors to capture intermediate image states

A typical experiment involves running several uniform halftone density prints of a particular color (C, M, Y or K) and logging the sensor data. Let $y_i(x)$ represent the measured image state i at location x in the process direction. If there are Q patches in every page and there are P pages in the print run, then x takes values from 1 to N, where $N=PQ$ is the total number of patches in the print run. Note that y_i may be thought of as time series representations of the image states.

The autocorrelation functions (A) and cross-correlation (C) functions can be written as [3]

$$A_i(\Delta p) = \sum_{p=1}^{N-\Delta p}\left[\frac{y_i(p)-\bar{y}_i}{\sigma_i}\right]\left[\frac{y_i(p+\Delta p)-\bar{y}_i}{\sigma_i}\right]$$
$$C_{ji}(\Delta p) = \sum_{p=1}^{N-\Delta p}\left[\frac{y_i(p)-\bar{y}_i}{\sigma_i}\right]\left[\frac{y_j(p+\Delta p)-\bar{y}_j}{\sigma_j}\right] \quad (1)$$

where Δp is called the lag, and $\bar{y}$ and σ is the mean and standard deviation of y, respectively. The autocorrelation function refers to correlation of a time series with its own past and future values and is especially useful in detecting periodic structures in the data. The cross-correlation refers to correlations between two time shifted time series and is useful to understand transient or delayed response to a common stimulus that impacts both time series. Cross-correlations are also useful to understand relationships between present values at sensor locations ($y_i(p)$) and future values at output locations ($y_j(p+\Delta p)$), which can be used to design process

controls. Note that detrending is sometimes needed as a preprocessing step to prepare the time series for analysis.

Correlation analyses assume linearity since the correlation coefficients measure the strength of linear association between the time series. Linearity is often a good assumption for variations that are sufficiently small. It is however applicable in the present context, since we are concerned with small variations about the mean in the image states, and how these variations propagate through the printing system. Let $\hat{y}_i$ and $\hat{y}_j$ be two normalized time series representing the image states at sensor locations *i* and *j*, where $\hat{y} = (y - \bar{y})/\sigma$ has zero mean and unit variance. Using linear system theory we can write

$$\hat{y}_j = \alpha \hat{y}_i + \sqrt{1-\alpha^2}\,\hat{n}_{ij} \qquad (2)$$

where is α the Pearson correlation coefficient $= \langle \hat{y}_j \hat{y}_i \rangle$ which signifies the fraction of variance in image state *j* due to variance in image state *i*. The second term in Eq. (2) signifies the component in $\hat{y}_j$ that is uncorrelated with $\hat{y}_i$. This can be interpreted as the noise ($\hat{n}_{ij}$) added by processes and subsystems between image states *i* and *j*, where $\hat{n}_{ij} = (\hat{y}_j - \alpha \hat{y}_i)/\sqrt{1-\alpha^2}$.

Results and Discussion

We now present some applications of the methodology discussed previously. Figure 2 shows a portion of the time series data of *Esv*, *Etac* (toner density sensor measuring specular reflectance) and *lStar* (measured offline using a spectrophotometer) for 50% Cyan halftone. For this print run, the number of patches per page, Q, is 10 and the number of pages, P, is 100. Note that the time series data has been normalized. For the *Etac* data, the clean belt signature needs to be removed for consistent results. We observe that some of the structure in *lStar* data is observed in the *Etac* data and *Esv* data. Note that the *Esv* data is negatively correlated to *Etac* and *lStar* (higher or less negative *Esv*, leads to higher toner mass or lower *Etac* and darker color or lower *lStar*). Figure 3 shows scatter plots of *Esv* versus *Etac* and *Etac* versus *lStar*. Scatter plots are useful to test assumptions of linearity. We note that *Etac* and *lStar* are well correlated (less scattered) when compared to *Esv* and *Etac* data.

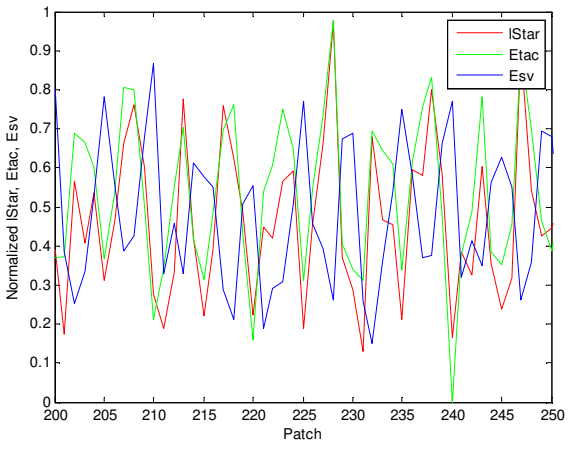

Figure 2: Portion of time series data showing variation in image states

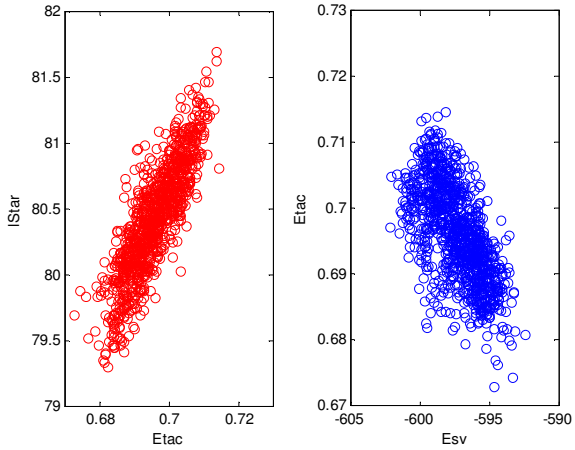

Figure 3: Scatter plots of Etac versus lStar (left) and Esv versus Etac (right)

Next we consider the autocorrelation of image states. Figure 4 shows the autocorrelations of *lStar, Etac* and *Esv*. We observe autocorrelation peaks at lags that are multiples of 5. This is consistent with a periodic defect such as banding. In this case, since the peaks show up in all three image states, we can surmise that it is be related to the imaging drum, and the lag of 5 is consistent with photoreceptor banding. Some aliasing is observed due to the low sampling rate used in the analysis. The values of the autocorrelation function at the peaks, can be used to quantify the contribution of particular sources to the overall variation. For instance, if R_1 is the autocorrelation at side lobe Δp_1, then R_1 is the fractional contribution of the source at Δp_1 to the overall variance.

Figure 5 shows the cross correlations between *lStar* and *Etac* and *Etac* and *Esv*. The side lobes (peaks) observed at non zero lags is due to photoreceptor banding. The square of the cross correlations at zero lag, $C_{ij}(0)$, signifies the fraction of variance in *j* explained by variance in *i*. Thus the fraction of variance in *lStar* due toner mass variance on the intermediate belt is $C_{Etac\text{-}lStar}(0)^2$ while the remainder $(1- C_{Etac\text{-}lStar}(0)^2)$ signifies the fraction of variance in *lStar* due to transfer and fusing processes. Similarly, the fraction of variance in toner mass on the intermediate belt due to voltage variations in the latent image is $C_{Esv\text{-}Etac}(0)^2$, while the

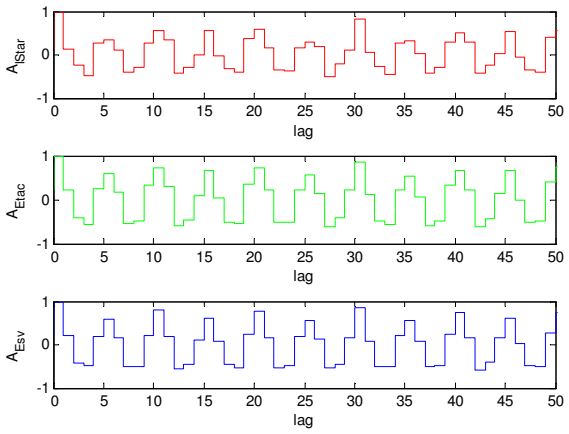

Figure 4: Autocorrelation of lStar, Etac and Esv

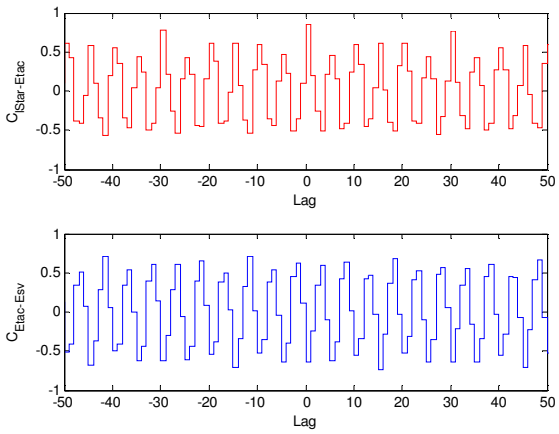

Figure 5: Cross correlations between *lStar* and *Etac* (top) and between *Etac* and *Esv* (bottom)

remainder $(1- C_{Esv\text{-}Etac}(0)^2)$ signifies the fractional contributions due to develop and first transfer/retransfer processes. Thus the cross correlations between image states can help to develop a pareto chart of the main drivers of the overall color stability. This procedure can be repeated under various system noises such as environment, component age and customer usage to understand the sensitivity of the main drivers to noises.

As an example of how correlation analyses can be used to understand sensitivity to noises, let us consider the impact of toner dispense rate on color stability. Print targets were generated that varied the cyan area coverage of the document outside the sensor locations, while the area coverage in the sensor location was maintained at 50% AC. This allows us to evaluate the color stability of 50% Cyan as a function of dispense rate. Figure 6 shows toner dispense rate for three print runs: low AC, nominal AC and high AC. The correlation analyses described previously was repeated for all three print runs. Figure 7 shows a pareto chart of the contributors to variance in *lStar* as a function of dispense rate. We observe that the overall variance in *lStar* increases for a high dispense rate. However, the fractional contribution from various subsystems stays about the same: ≈25% for Charge, Expose and PIDC; ≈50% for Develop, 1st Transfer and Retransfer; and ≈25% for 2nd Transfer and Fusing. A finer partitioned pareto chart detailing contributions from each component or subsystem is possible if additional intermediate image states are captured.

Conclusions

This paper discussed methodologies based on correlation analyses to help diagnose color stability in printing systems. Examples were presented to illustrate the application of the methodologies to help identify drivers of color variation in the xerographic process. Knowledge of the drivers and their relative importance can help suggest approaches to decrease color variation, such as through improving subsystem performance or improving process controls.

References

[1] M. Neilsen et. al., "A method for assessing the color stability requirements for a printing device", ICIS '06, 99-102 (2006).

[2] L.K. Mestha, "Control engineering for color printing," Proc. 1996 IEEE Int. CCA, 759-763, (1996).

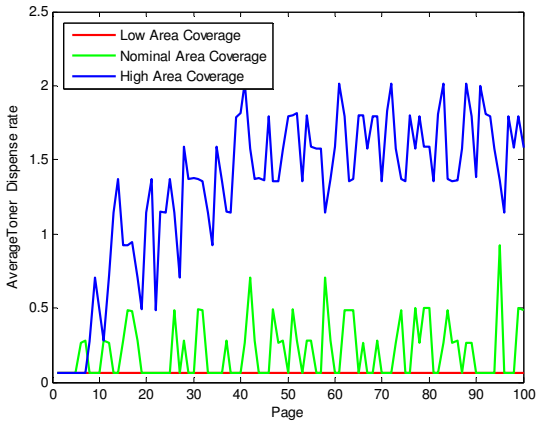

Figure 6: Toner dispense rate as a function of area coverage

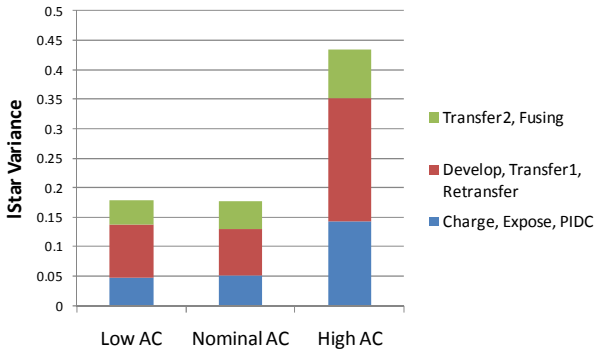

Figure 7: Pareto of contributors to variance of lStar versus Area Coverage

[3] S.J. Orfanidis, Optimum Signal Processing. An Introduction. 2nd Edition, Prentice-Hall, Englewood Cliffs, NJ, (1996).

Author Biography

Palghat Ramesh received his BTech in Mechanical Engineering from IIT Madras, India in 1982 and PhD in Mechanical Engineering from Cornell University in 1988. Since joining Xerox in 1989, his focus has been in the areas of xerographic process modeling and simulation. He is currently a Principal Scientist with the Xerox Innovation Group. Ramesh is the author of 14 US patents and more than 40 external publications.

Peter Paul received his BS, MS, and PhD degrees in Electrical Engineering from Case Western Reserve University in 1990, 1991, and 1994, respectively. After completing his PhD, he joined the technical staff at Hughes Aircraft Company working on adaptive beamforming and other advanced signal and image processing technologies applied to radar systems. Since joining Xerox in 1999 he has been a member of the Xerox Innovation Group, becoming a Principal Scientist in 2006. Peter's focus is on systems and controls, and signal and image processing. He is the author of 16 patents in these areas.

Eric Gross received his BS in Mechanical Engineering from Rensselaer Polytechnic Institute in 1986, and was employed at the Aerospace Corporation from 1987 until 1989. He completed his PhD in Dynamic Systems and Control from the UC Berkeley in 1993 and spent 4 years on the technical staff at the Toshiba Center for Manufacturing Research in Isogo, Japan. Eric joined Xerox in 1997 and is currently in the Xerox Innovation Group, Webster. Eric's focus is systems integration and control. He is the author of more than 28 patents related to xerographic control systems technology.